4.1 DOPPLER LIDAR MEASUREMENTS OF HIGHER-ORDER VERTICAL VELOCITY STATISTICS IN THE CONVECTIVE BOUNDARY LAYER

Donald H. Lenschow[1]*, Marie Lothon[2], and Shane D. Mayor[3]

[1]National Center for Atmospheric Research, Boulder, CO
[2] Université de Toulouse, Laboratoire d' Aérologie – CNRS UMR 5560, Toulouse, France
[3]Department of Geosciences and Department of Physics, California State University, Chico, CA

1. MOTIVATION

Higher-order velocity statistics can provide useful information about the structure of turbulence in the convective boundary layer (CBL). Profiles of velocity variance are commonplace, but say nothing about how the turbulence departs from *e.g.* a Gaussian distribution. Moments higher than two can provide this information, but with a considerable increase in random (sampling) error (Lenschow et al., 1994). That is, for the same relative statistical significance, a considerably longer measurement time is required for moments greater that two. This is one reason why there are fewer measurements of moments greater than two reported in the literature.

Doppler lidar is one tool that can be used to address the sampling issue. The lidar can point in a particular direction for long periods of time and measure the radial velocity component of aerosol particles in each sampling volume along the beam. Thus, a line of simultaneous velocity measurements can be obtained along the beam.

We describe here the deployment of the 2.022 μm wavelength High Resolution Doppler Lidar (HRDL) developed by the NOAA Environmental Technology Laboratory and described by Grund et al. (1998) during the Lidars in Flat Terrain (LIFT) experiment. HRDL was pointed straight up for extended periods of time on twelve days for a total of 110 h to measure the vertical velocity w in the CBL between 26 July and 22 August 1996. It operated at a pulse repetition rate of 200 s^{-1} in the zenith-pointing mode over level farmland (a patchwork of corn and soybean fields) in central Illinois. The spatial resolution was about 30 m and the distance from the lidar to the first detectable velocity signal ("dead zone") was about 390 m. The lidar vertical range extended to the top of the CBL but not above—except for one case—because of the reduced aerosol content of the free troposphere. However, above about $0.75z_i$, where z_i is the CBL depth, the lidar signal occasionally dropped out, likely due to entrainment of low-backscatter parcels from the overlying free troposphere, which limits the effective vertical range of the w measurement.

We discuss here the second- third-, and fourth-order moments of w from about 390 m above the surface to the top of the CBL. We use Taylor's hypothesis to convert the time series into the spatial domain using the mean horizontal wind U. Profiles of U were obtained from a wind profiler located at Sadorus, IL, about 5 km from the HRDL . The resulting vertical cross-sections were used to calculate moments of w as a function of height z with unprecedented vertical resolution throughout the mid-region of the CBL. We compare the observed statistics for eleven cases centered about mid-afternoon (from about 1300 LT to 1600 LT) with previous formulations based on both measurements and numerical simulations, and discuss the differences, both on an averaged and a case-by-case basis. Details of the experiment and of the corollary experiment, the Flatlands Experiment, are presented in Angevine et al. (1998), Cohn et al. (1998), and Lothon et al. (2006).

2. RESULTS

Here we show profiles of the second- through fourth-order moments of w. The moments have all been corrected for uncorrelated noise using the technique developed by Lenschow et al. (2000), but the noise contribution is small. Table 1 lists the defining parameters for the eleven LIFT cases, including details of both the mean and turbulence structure, and the transition to the overlying free troposphere.

Figure 1 shows the velocity variances σ_w^2 as a function of normalized height $z_* = z/z_i$ for all eleven LIFT cases. In this and the succeeding figures, the red symbols are the most convective cases ($\zeta \equiv -z_i/L_o > 30$) and the blue the least unstable ($\zeta < 30$). The smoothed curves are weighted averages; that is, they were obtained by applying a weighting factor to each case to take into account the sample length of each case, which is the product of U times the sample period. The curves all show a maximum variance at about 0.3 to 0.4 z_i, which is in agreement with previous observations (*e.g.* Lenschow et al. (1980)). Not

*Corresponding address: Donald H. Lenschow, National Center for Atmospheric Research, P. O. Box 3000, Boulder, CO, 80307-3000. E-mail: lenschow@ucar.edu

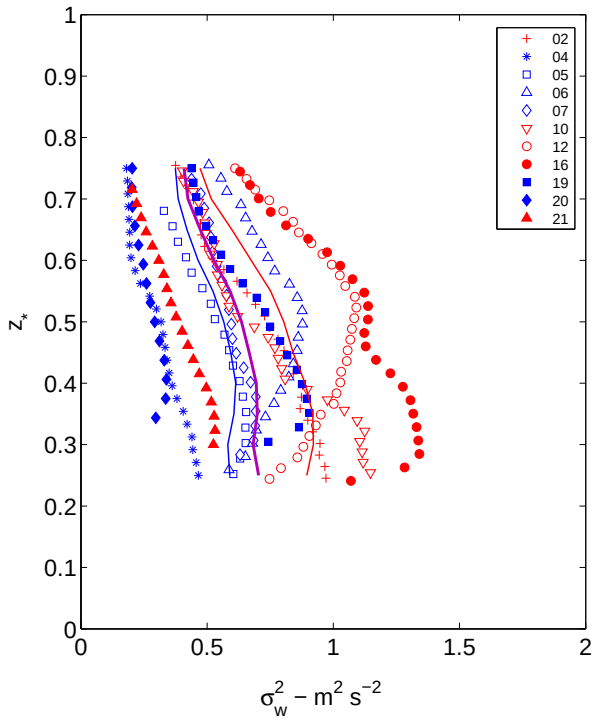

Figure 1: Profiles of vertical velocity variance measured by HRDL in the CBL during LIFT. The symbols identify the dates (in August, 1996) of the eleven cases, as described in Table 1. The smoothed colored curves are averages of the observations; the red curve and symbols are the most unstable cases, the blue curve and symbols the least unstable, and the magenta curve the overall weighted average.

surprisingly, on average the most unstable cases have the largest variances.

Figure 2 shows the variances normalized by w_*^2 where

$$w_* = \left(\frac{g}{T}\langle w\theta\rangle_0 z_i\right)^{1/3} \tag{1}$$

is the convective velocity scale, g is gravity, T is the mean CBL temperature, $\langle w\theta\rangle_0$ is the surface virtual potential temperature flux, and z_i is the CBL depth. $\langle w\theta\rangle_0$ was obtained from Flux-PAM (Portable Automated Mesonet) surface flux measurement stations deployed in the Flatlands Experiment (Angevine et al., 1998) within a few kilometers of the HRDL site. As expected, the normalization collapses the cases, so that on average there is no significant variation with ζ.

We also show comparisons with the large-eddy simulation (LES) results of Sullivan and Patton (2008). The values of ζ for the three LES cases presented in the figures are as follows: most shear (least convective), $\zeta = 5.9$, more shear, $\zeta = 19.5$, and least shear (most convective), $\zeta = 684$. This range encompasses all the observed values encountered in LIFT. The LES results also show little variation with ζ, and agree well with the general shape of the LIFT curves and with the previous aircraft observations of Lenschow et al. (1980) during the Air Mass Modification Experiment (AMTEX) with cold-air outbreaks over the East China Sea, which follow the relation plotted in Figure 2,

$$\frac{\langle w^2\rangle}{w_*^2} = 1.8 z_*^{2/3}(1-0.8z_*)^2, \tag{2}$$

where $z_* = z/z_i$. The aircraft observations also agree with tethered-balloon observations over uniform terrain during the Minnesota Experiment (Kaimal et al., 1976). However, the LIFT curves are about 15% less than the LES results and the previous observations. We do not know why, but one possibility may be that because the LIFT site is not as horizontally homogeneous as the previous observations and the LES case, the fixed-point buoyancy-flux estimates here may not be representative of the area average. This is further supported by the averaged normalized third-moment observations $\langle w^3\rangle/w_*^3$ (not shown), which are about 20% less than the LES values.

Figure 3 shows profiles of the w skewness,

$$S \equiv \frac{\langle w\rangle^3}{\sigma_w^3}. \tag{3}$$

We see that on average the modeled and observed values of S are in good agreement, but that the observations show a considerably larger change with stability than the modeled values of S. For example, the most convective case (16 August) has a maximum $S \simeq 1.5$. We note, however, that 16 August is a light-wind case, which means that the sampling statistics are poorer than for other cases. In Figure 4, we see that the LIFT observations are also in agreement with previous observations of S reported by Lenschow et al. (1980) over the ocean and Wyngaard (1988) over a homogeneous land surface. However, in the upper half of the CBL, the LES values continue to increase up to near the CBL top, while the previous observations show a maximum of $S \simeq 0.6-0.7$ in the middle of the CBL and slight decrease with height above. The LIFT results are consistent with the previous observations in showing no signs of a monotonic increase with height in the limited region that they extend into the upper part of the CBL. Sullivan and Patton (2008) discuss reasons for this apparent overestimation of skewness by LES in the upper part of the CBL.

Figure 5 shows profiles of the w kurtosis, defined by

$$K \equiv \frac{\langle w\rangle^4}{\sigma_w^4}. \tag{4}$$

Table 1: Mean characteristics of the 11 LIFT cases considered here. θ_{v_m} and r_{v_m} are the mean virtual potential temperature and water vapor mixing ratio in the mixed layer, w_* is the convective velocity scale, u_* is the friction velocity, $\Delta\theta_v$ and $\Delta U = \sqrt{\Delta u^2 + \Delta v^2}$ are jumps across the inversion, γ is the lapse rate above the CBL, $\zeta = -z_i/L_o$, where L_o is the Monin-Obukhov length, χ is the cloud fraction, and l_w and λ_w are respectively the observed along-wind (transverse) integral scale and the wavelength λ_w at which the w energy density spectrum reaches its maximum, both evaluated at $z_i/2$ and normalized by z_i in the table.

Date (1996)	z_i m	U m s^{-1}	θ_{v_m} K	r_{v_m} g kg^{-1}	w_* m s^{-1}	u_* m s^{-1}	$\Delta\theta_v$ K	ΔU m s^{-1}	γ K km^{-1}	ζ	χ	l_w/z_i	λ_w/z_i
2 Aug	1590	3.0	299.8	9.8	1.58	0.16	1.16	1.0	4.7	407	0.47	0.14	0.85
4 Aug	1440	5.2	302.9	10.9	1.23	0.35	/	1.8	2.0	17	0.26	0.14	0.81
5 Aug	1190	8.6	306.7	14.7	1.34	0.52	1.86	5.8	2.4	7	0.28	0.13	0.78
6 Aug	1390	7.8	307.7	13.1	1.36	0.46	1.16	1.0	5.9	10	0.20	0.33	4.19
7 Aug	1270	5.6	308.7	15.6	1.29	0.39	0.35	2.2	1.8	14	0.28	0.25	2.33
10 Aug	1770	2.2	299.6	8.3	1.55	0.39	2.32	2.9	7.6	220	0.21	0.18	1.26
12 Aug	1720	4.8	300.8	10.7	1.56	0.19	1.16	1.1	2.6	37	0.41	0.29	1.79
16 Aug	1370	2.2	298.8	8.2	1.62	0.34	4.88	4.1	1.6	236	0.17	0.29	1.85
19 Aug	1280	7.2	304.1	11.8	1.55	0.19	3.95	2.9	1.0	9	0.21	0.24	2.33
20 Aug	960	6.8	305.5	14.8	1.14	0.43	1.63	3.1	1.2	8	0.05	0.18	1.46
21 Aug	1300	3.4	305.6	11.5	1.20	0.26	0.7	0.9	1.3	41	0.13	0.23	1.61

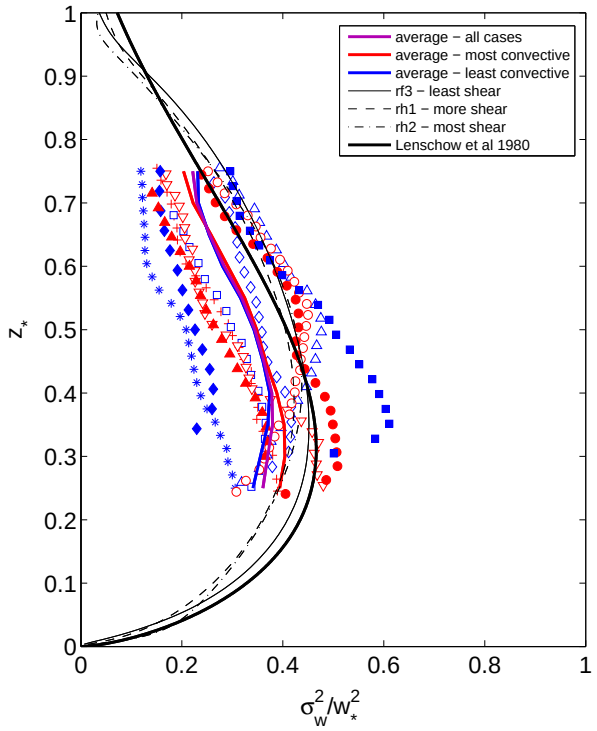

Figure 2: Profiles of normalized vertical velocity variance in the CBL. The symbols are lidar measurements from LIFT defined in Figure 1. The smoothed colored curves are averages of the observations and the thin black lines are LES simulations (Sullivan and Patton, 2008).

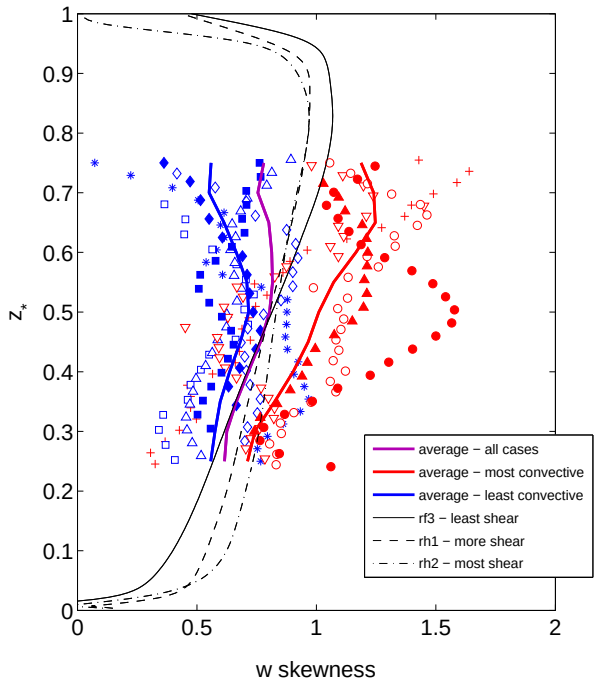

Figure 3: Profiles of vertical velocity skewness in the CBL. The symbols are lidar measurements from LIFT defined in Figure 1. The smoothed colored curves are averages of all the observations and the black lines are LES simulations (Sullivan and Patton, 2008).

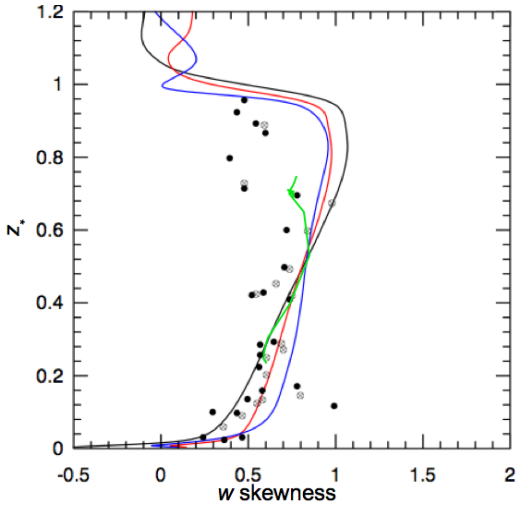

Figure 4: Profiles of vertical velocity skewness in the CBL. The symbols are observations from previous experiments, as described by Moeng and Rotunno (1990), and the green line is the mean of the LIFT observations. The black (least shear), red (more shear) and blue (most shear) curves are LES results (Sullivan and Patton, 2008).

Again, the LIFT results are in good agreement with the LES results on average, but the LIFT observations show more variation with stability. The most convective (lightest wind) case, 16 August, has a considerably larger kurtosis in the middle of the CBL, similar to the skewness for this case. Except for 16 August, both the LES and the averaged LIFT results show a gradual increase with height, from a value close to the Gaussian K of three up to $z_* \simeq 0.4$ to values > 4 in the upper part of the CBL.

Lenschow et al. (1994) modeled a non-Gaussian process by modifying a Gaussian process $\tilde{z}(t)$ with variance σ_z and an exponential autocorrelation function such that

$$\tilde{w}(t) \equiv \tilde{z}(t) + a\frac{\tilde{z}^2(t) - \langle \tilde{z}^2(t) \rangle}{\sigma_z}, \qquad (5)$$

where a is a constant that determines the departure of $\tilde{w}(t)$ from a Gaussian distribution. The skewness and kurtosis of this modified Gaussian process are:

$$\tilde{S} = \frac{2a(3+4a^2)}{(1+2a^2)^{3/2}} \qquad (6)$$

$$\tilde{K} = \frac{3(1+20a^2+20a^4)}{(1+2a^2)^2} \qquad (7)$$

Figure 6 shows a parametric curve of skewness vs. kurtosis based on this model, along with the LIFT and LES results. The observations are a reasonable fit to the model, especially for the most convective cases; similarly, the LES results are in reasonable agreement with

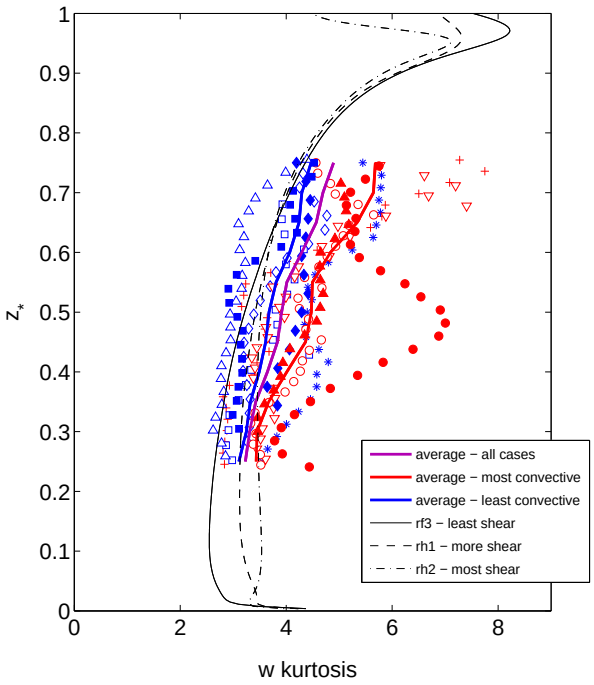

Figure 5: Profiles of vertical velocity kurtosis in the CBL. The symbols are lidar measurements from LIFT defined in Figure 1. The smoothed colored curves are averages of the observations and the black lines are LES simulations (Sullivan and Patton, 2008).

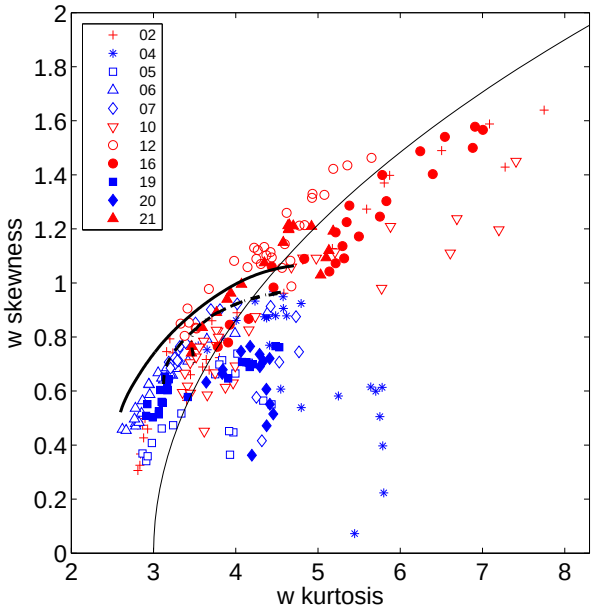

Figure 6: Parametric curve of skewness vs kurtosis (thin solid line). The symbols are HRDL measurements from LIFT. The thick black lines are LES simulations (Sullivan and Patton, 2008), with the solid line being the "least shear" and the dashed line the "more shear" cases.

the model, with the least convective (most shear) case being somewhat closer to the model than the more convective (most shear) case.

3. DISCUSSION

Figure 7 shows plots of S averaged over $0.4 < z_* < 0.6$ versus $\zeta^{1/3}$ (left panel) and u_* (right panel). We see that with the exception of two very convective cases (2 August and 10 August), S increases with convective instability and decreases with u_*. This illustrates more directly the stronger variation of the LIFT observations with stability than the LES results. 2 August has the largest cloud fraction of all the cases, which may be a complicating factor here since cloud downdrafts may generate negative skewness. Furthermore, both of the exceptions show a rapid increase in S at higher levels, so that they merge with the other more convective cases, and they both have very light mean winds, which means that the samples are statistically less significant than for most other cases. We do not observe any obvious correlation between shear at the top and skewness in the middle of the PBL (not shown).

These results show the unique ability of Doppler lidar to measure turbulence statistics of w simultaneously throughout much of the CBL. Long time series of w can be collected at 30 m height increments throughout the middle of the CBL. They also indicate obvious limitations in the HRDL at the time of the LIFT deployment that, if addressed, could make the system even more useful. Namely, the dead zone eliminates observations below about 390 m, and sensitivity limitations typically eliminate observations in the entrainment zone and above. One possibility for eliminating the dead zone may be to point the lidar horizontally at a mirror located $>$ 390 m away that redirects the beam vertically. Of course, measurements closer to the ground will be increasingly affected by the decreasing integral length scale of w as z decreases.

Increasing the detector sensitivity and the lidar pulse energy could potentially increase the range. Finally, in LIFT the HRDL concentrated on w measurements. It could also be used to collect long time series of horizontal velocity components by pointing horizontally from various heights within the CBL, either by deploying the lidar at various heights, or by mounting a mirror at various heights that reflects a vertical beam to the horizontal.

Acknowledgements

The LIFT project was funded by the NCAR Atmospheric Technology Division Director's Office and the Department of Energy/OAGR. This work was made possible thanks to the support of the Mesoscale and Microscale Meteorology Division and the Earth Observing Laboratory of NCAR. We thank Peter Sullivan, Ned Patton, and Wayne Angevine for their assistance during the course of this work.

REFERENCES

Angevine, W. M., A. W. Grimsdell, L. M. Hartten, and A. C. Delany, 1998: The Flatland Boundary Layer Experiments, *Bull. Amer. Meteor. Soc.*, **79**, 419–431.

Cohn, S. A., S. D. Mayor, T. M. Grund, T. M. Weckwerth, and C. Senff, 1998: The Lidars In Flat Terrain Experiment (LIFT), *Bull. Amer. Meteor. Soc.*, **79**, 1329–1343.

Grund, C. J., R. M. Banta, J. George, J. N. Howell, M. J. Post, and R. A. Richter, 1998: High-resolution Doppler lidar for boundary layer and cloud research, *J. Atmos. Oceanic Technol.*, **18**, 376–393.

Kaimal, J. C., J. C. Wyngaard, D. A. Haugen, O. R. Coté, and Y. Izumi, 1976: Turbulence structure in the convective boundary layer, *J. Atmos. Sci.*, **33**, 2152–2169.

Lenschow, D. H., J. Mann, and L. Kristensen, 1994: How long is long enough when measuring fluxes and other turbulence statistics?, *J. Atmos. Oceanic Technol.*, **11**, 661–673.

Lenschow, D. H., V. Wulfmeyer, and C. Senff, 2000: Measuring second- through fourth-order moments in noisy data, *J. Atmos. Oceanic Technol.*, **17**, 1330–1347.

Lenschow, D. H., J. C. Wyngaard, and W. T. Pennell, 1980: Mean-field and second-moment budgets in a baroclinic, convective boundary layer, *J. Atmos. Sci.*, **37**, 1313–1326.

Lothon, M., D. H. Lenschow, and S. D. Mayor, 2006: Coherence and scale of vertical velocity in the convective boundary layer from a Doppler lidar, *Boundary-Layer Meteorol.*, **121**, 521–536.

Moeng, C.-H. and R. Rotunno, 1990: Vertical velocity skewness in the buoyancy-driven boundary layer, *J. Atmos. Sci.*, **47**, 1149–1162.

Sullivan, P. P. and E. G. Patton, 2008: A highly parallel algorithm for turbulence simulations in planetary boundary layers: Results with meshes up to 1024^3, in *18th Symposium on Boundary Layer and Turbulence*, 9–13 June 2008, Stockholm, Sweden.

Wyngaard, J., 1988: Structure of the PBL, in *Lectures on Air Pollution Modeling*, edited by A. Venkatram and J. Wyngaard, p. 385, Americ. Meteor. Soc., Boston, MA.

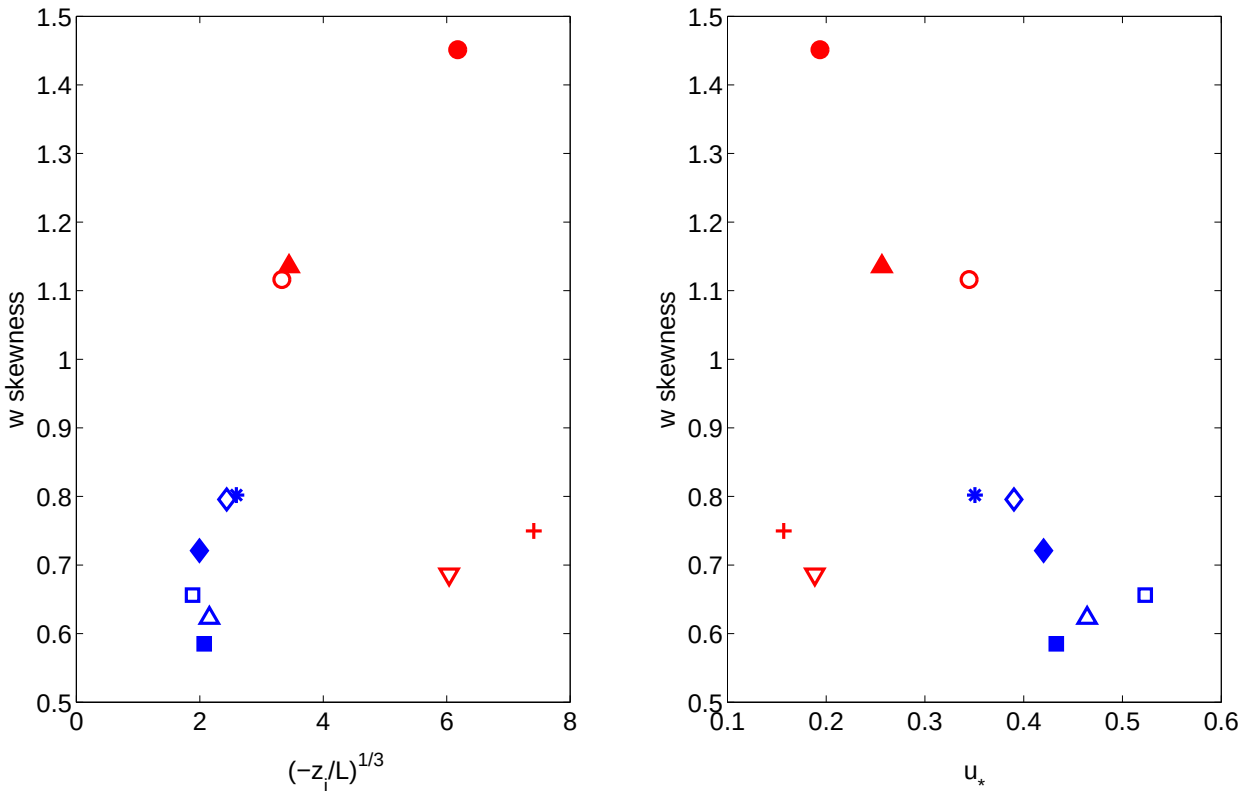

Figure 7: Observations of w skewness at $z_i/2$ as functions of $\zeta^{1/3}$ (left) and friction velocity u_* (right). blue symbols are for the less convective and red symbols for the more convective cases. The symbols are defined in Figure 1.